NEIGHBORING EXTREMAL OPTIMAL CONTROL DESIGN INCLUDING MODEL MISMATCH ERRORS

Theodore J. Kim* and David G. Hull†

Abstract

The mismatch control technique that is used to simplify model equations of motion in order to determine analytic optimal control laws is extended using neighboring extremal theory. The first variation optimal control equations are linearized about the extremal path to account for perturbations in the initial state and the final constraint manifold. A numerical example demonstrates that the tuning procedure inherent in the mismatch control method increases the performance of the controls to the level of a numerically-determined piecewise-linear controller.

Nomenclature

a_γ - f_γ	linearization coefficients for trig functions
C_D	aerodynamic drag coefficient
C_{D_0}	zero-lift drag coefficient
C_L	aerodynamic lift coefficient
C_L^*	lift coefficient for maximum lift/drag ratio
E^*	maximum lift/drag ratio
h	altitude (ft)
h_R	density scale height (ft)
l	sweep variable
M	tuning parameter matrix
$\boldsymbol{m}$, $\boldsymbol{n}$	sweep variable matrices
$\boldsymbol{p}$	Lagrange multiplier vector
$\boldsymbol{Q}$, $\boldsymbol{R}$, $\boldsymbol{S}$	sweep variable matrices
t	time (sec)
$\boldsymbol{u}$	aerodynamic control vector
V	velocity (ft/sec)
w	mismatch control vector
$\boldsymbol{x}$	state vector
X	downrange distance (nm)
Y	crossrange distance (nm)
z	running variable
γ	flight path angle
η	nondimensional crossrange
λ	scaled lift coefficient
μ	Lagrange multiplier
ν	nondimensional velocity
ξ	nondimensional downrange
ρ	air density (slugs/ft^2)
σ	scaled side force coefficient
χ	track angle
ψ	final constraint manifold
ω	nondimensional density
Ω	end point function

*Senior Member of the Technical Staff, Aided Navigation and Remote Sensing Department, Sandia National Laboratories, Albuquerque, NM. Member AIAA.

†M.J. Thompson Regents Professor, Department of Aerospace Engineering and Engineering Mechanics, The University of Texas, Austin, TX. Associate Fellow AIAA.

Introduction

Optimal control theory that is derived from Newton's calculus of variations [1] is often used to compute a control law. However, this control is the solution of a two point boundary value problem (TPBVP) that is usually nonlinear and can only be solved numerically. The mismatch controls that are defined in [2] reduce the complexity of the differential equations of motion that describe a physical system. The resulting model equations of motion simplify the TPBVP and often admit an analytic solution for the controls.

The general optimal control problem that includes the mismatch controls is written

$$\underset{\mathbf{w}}{\text{ext}}\ \underset{\boldsymbol{u}}{\min}\ J \tag{1}$$

where w denotes the mismatch controls and $\boldsymbol{u}$ denotes the "normal" controls. (In this paper, $\boldsymbol{u}$ will be called the aerodynamic controls.) The mismatch controls extremize (either minimize or maximize) the performance index, J, hence the nonstandard notation "ext". The performance index for this problem is

$$J = \phi(t_f, \boldsymbol{x}_f) + \int_{t_0}^{t_f} \left[\mathcal{L}(t, \boldsymbol{x}, \boldsymbol{u}) + \frac{1}{2}\mathbf{w}^T M^{-1}\mathbf{w}\right] dt \tag{2}$$

where the matrix M is a diagonal matrix of constants. These constants are the tuning parameters that are associated with the mismatch controls. The tuning parameters are user-selected by tuning the control solution against the true vehicle dynamics during computer simulations of the control law.

If the performance index is separable in $\boldsymbol{u}$ and $\mathbf{w}$, the control solution is independent of the order of optimization [3] and the first variation conditions that describe the extremal path are

$$\frac{d\boldsymbol{x}}{dt} = \bar{\boldsymbol{f}}(t,\boldsymbol{x},\boldsymbol{u}) + \mathbf{w} \quad (3)$$

$$\frac{d\boldsymbol{p}}{dt} = -H_{\boldsymbol{x}}^T(t,\boldsymbol{x},\boldsymbol{u},\mathbf{w},\boldsymbol{p}) \quad (4)$$

$$0 = H_{\boldsymbol{u}}^T(t,\boldsymbol{x},\boldsymbol{u},\boldsymbol{p}) \quad (5)$$

$$0 = H_{\mathbf{w}}^T(t,\boldsymbol{x},\mathbf{w},\boldsymbol{p}). \quad (6)$$

In the above equations, t is the time, $\boldsymbol{x}$ is the state vector, $\boldsymbol{p}$ is the Lagrange multiplier vector, $\bar{\boldsymbol{f}}$ is the approximate state vector, and H is the Hamiltonian. The Hamiltonian for this problem is

$$H = \mathcal{L}(t,\boldsymbol{x},\boldsymbol{u}) + \frac{1}{2}\mathbf{w}^T\mathbf{M}^{-1}\mathbf{w} + \boldsymbol{p}^T[\bar{\boldsymbol{f}}(t,\boldsymbol{x},\boldsymbol{u}) + \mathbf{w}] \quad (7)$$

and is separable in $\boldsymbol{u}$ and $\boldsymbol{w}$. The boundary conditions for the extremal differential equations are

$$t_0,\ \boldsymbol{x}_0 \text{ specified} \quad (8)$$

$$\boldsymbol{\psi}(t_f,\boldsymbol{x}_f) = 0 \quad (9)$$

$$\Omega(t_f,\boldsymbol{x}_f,\boldsymbol{u}_f,\mathbf{w}_f,\boldsymbol{\mu}) \triangleq \mathcal{L}_f + G_{\boldsymbol{x}_f}\boldsymbol{f}_f + G_{z_f} = 0 \quad (10)$$

$$\boldsymbol{p}_f = G_{\boldsymbol{x}_f}^T(t_f,\boldsymbol{x}_f,\boldsymbol{\mu}) \quad (11)$$

where G is the Bolza function, Ω is the end point function, and $\boldsymbol{\psi}$ is the final constraint manifold. These equations along with Eqs. (3) - (6) define the TPBVP which yield the extremal controls.

A necessary condition for the optimality of the extremal controls is the Legendre-Clebsch condition, which checks the sign of the second derivative of the Hamiltonian with respect to the controls. For the aerodynamic controls to be minimal,

$$H_{\boldsymbol{u}\boldsymbol{u}}(t,\boldsymbol{x},\boldsymbol{u},\boldsymbol{p}) \geq 0, \quad (12)$$

which can only be checked when the specific problem has been defined. However,

$$H_{\mathbf{w}\mathbf{w}} = \mathbf{M}^{-1}, \quad (13)$$

so the sign of the individual tuning parameters determine whether the mismatch controls minimize or maximize the performance index.

Neighboring Extremal Controls

A neighboring extremal (NE) path is a path that lies in the neighborhood of the extremal path and satisfies the first variation conditions [1]. The equations that describe this path are found by linearizing the extremal equations and boundary conditions about the extremal path. Even though it is not known whether the mismatch controls minimize or maximize the performance index, the NE path can be determined.

In general, the neighboring extremal path originates at a perturbed initial state, $\tilde{\delta}\boldsymbol{x}_0$, and ends at a perturbed value of the final constraint manifold, $\boldsymbol{\psi} + \delta\boldsymbol{\psi}$. The symbol $\tilde{\delta}\boldsymbol{x}_0$ denotes a time-constant variation of the initial state, while $\delta\boldsymbol{\psi}$ refers to the total change in $\boldsymbol{\psi}$. The relationship between fixed and total variations is

$$\delta(\ )_* = \tilde{\delta}(\ )_* + \left.\frac{d(\ )}{dt}\right|_* \delta t_* \quad (14)$$

where t_* is any value between t_0 and t_f.

By linearizing Eqs. (3) - (6) about the optimal path, the neighboring extremal equations are determined to be

$$\frac{d}{dt}\left(\tilde{\delta}\boldsymbol{x}\right) = f_{\boldsymbol{x}}\tilde{\delta}\boldsymbol{x} + f_{\boldsymbol{u}}\tilde{\delta}\boldsymbol{u} + f_{\mathbf{w}}\tilde{\delta}\mathbf{w} \quad (15)$$

$$\frac{d}{dt}\left(\tilde{\delta}\boldsymbol{p}\right) = -H_{\boldsymbol{x}\boldsymbol{x}}\tilde{\delta}\boldsymbol{x} - H_{\boldsymbol{x}\boldsymbol{u}}\tilde{\delta}\boldsymbol{u} - H_{\boldsymbol{x}\mathbf{w}}\tilde{\delta}\mathbf{w} - f_{\boldsymbol{x}}^T\tilde{\delta}\boldsymbol{p} \quad (16)$$

$$0 = H_{\boldsymbol{u}\boldsymbol{x}}\tilde{\delta}\boldsymbol{x} + H_{\boldsymbol{u}\boldsymbol{u}}\tilde{\delta}\boldsymbol{u} + f_{\boldsymbol{u}}^T\tilde{\delta}\boldsymbol{p} \quad (17)$$

$$0 = H_{\mathbf{w}\boldsymbol{x}}\tilde{\delta}\boldsymbol{x} + H_{\mathbf{w}\mathbf{w}}\tilde{\delta}\mathbf{w} + f_{\mathbf{w}}^T\tilde{\delta}\boldsymbol{p} \quad (18)$$

where the substitutions $H_{\boldsymbol{x}\boldsymbol{p}} = f_{\boldsymbol{x}}^T$, $H_{\boldsymbol{u}\boldsymbol{p}} = f_{\boldsymbol{u}}^T$, and $H_{\mathbf{w}\boldsymbol{p}} = f_{\mathbf{w}}^T$ have been made using the definition of the Hamiltonian, Eq. (7). For convenience, an augmented control vector is defined as $\bar{\boldsymbol{u}}^T = [\boldsymbol{u}\ \mathbf{w}]$. Eqs. (17) and (18) are rewritten more compactly as

$$0 = H_{\bar{\boldsymbol{u}}\boldsymbol{x}}\tilde{\delta}\boldsymbol{x} + H_{\bar{\boldsymbol{u}}\bar{\boldsymbol{u}}}\tilde{\delta}\bar{\boldsymbol{u}} + f_{\bar{\boldsymbol{u}}}^T\tilde{\delta}\boldsymbol{p} \quad (19)$$

where

$$H_{\bar{\boldsymbol{u}}\boldsymbol{x}} = \begin{bmatrix} H_{\boldsymbol{u}\boldsymbol{x}} \\ H_{\mathbf{w}\boldsymbol{x}} \end{bmatrix}, \quad f_{\bar{\boldsymbol{u}}}^T = \begin{bmatrix} f_{\boldsymbol{u}}^T \\ f_{\mathbf{w}}^T \end{bmatrix}, \quad (20)$$

$$H_{\bar{\boldsymbol{u}}\bar{\boldsymbol{u}}} = \begin{bmatrix} H_{\boldsymbol{u}\boldsymbol{u}} & \mathbf{0} \\ \mathbf{0} & H_{\mathbf{w}\mathbf{w}} \end{bmatrix}. \quad (21)$$

If $H_{\bar{\boldsymbol{u}}\bar{\boldsymbol{u}}}$ is nonsingular, the control perturbation can be solved from Eq. (19) as

$$\tilde{\delta}\bar{\boldsymbol{u}} = -H_{\bar{\boldsymbol{u}}\bar{\boldsymbol{u}}}^{-1}\left(H_{\bar{\boldsymbol{u}}\boldsymbol{x}}\tilde{\delta}\boldsymbol{x} + f_{\bar{\boldsymbol{u}}}^T\tilde{\delta}\boldsymbol{p}\right). \quad (22)$$

This solution is used to eliminate the control perturbation in Eqs. (15) and (16) so that the differential equations for $\tilde{\delta}\boldsymbol{x}$ and $\tilde{\delta}\boldsymbol{p}$ become

$$\tilde{\delta}\boldsymbol{x}' = \boldsymbol{A}\tilde{\delta}\boldsymbol{x} - \boldsymbol{B}\tilde{\delta}\boldsymbol{p} \quad (23)$$

$$\tilde{\delta}\boldsymbol{p}' = -\boldsymbol{C}\tilde{\delta}\boldsymbol{x} - \boldsymbol{A}^T\tilde{\delta}\boldsymbol{p} \quad (24)$$

DISCLAIMER

Portions of this document may be illegible in electronic image products. Images are produced from the best available original document.

where

$$A = f_x - f_{\bar{u}} H_{\bar{u}\bar{u}}^{-1} H_{\bar{u}x} \quad (25)$$
$$B = f_{\bar{u}} H_{\bar{u}\bar{u}}^{-1} f_{\bar{u}}^T \quad (26)$$
$$C = H_{xx} - H_{x\bar{u}} H_{\bar{u}\bar{u}}^{-1} H_{\bar{u}x}. \quad (27)$$

The boundary conditions, Eqs. (8) - (11), are also linearized around the optimal path to obtain

$$z_0,\ \tilde{\delta}x_0 \text{ specified} \quad (28)$$
$$\delta\psi = \psi'_f \delta z_f + \psi_{x_f} \delta x_f \quad (29)$$
$$0 = \Omega'_f \delta z_f + \Omega_{x_f} \delta x_f + \Omega_\mu \delta\mu \quad (30)$$
$$\delta p_f = G_{x_f z_f} \delta z_f + G_{x_f x_f} \delta x_f + G_{x_f \mu} \delta\mu \quad (31)$$

since $\delta\Omega = 0$ and

$$\Omega_{\bar{u}_f} = \mathcal{L}_{\bar{u}_f} + G_{x_f} f_{\bar{u}_f} \quad (32)$$
$$= \mathcal{L}_{\bar{u}_f} + p_f^T f_{\bar{u}_f} = H_{\bar{u}_f} = 0. \quad (33)$$

The total variations of the states and the Lagrange multipliers at the final point z_f are replaced by the corresponding fixed variations using Eq. (14). The boundary conditions are now rewritten in matrix form as

$$\begin{bmatrix} \tilde{\delta}p_f \\ \delta\psi \\ 0 \end{bmatrix} = \begin{bmatrix} G_{x_f x_f} & \psi_{x_f}^T & \Omega_{x_f}^T \\ \psi_{x_f} & 0 & \psi'_f \\ \Omega_{x_f} & (\psi'_f)^T & \Omega'_f \end{bmatrix} \begin{bmatrix} \tilde{\delta}x_f \\ \delta\mu \\ \delta z_f \end{bmatrix} \quad (34)$$

by applying the following substitutions:

$$\Omega_\mu = \psi_{x_f} \quad (35)$$
$$G_{x_f \mu} = \psi_{x_f}^T \quad (36)$$
$$\Omega'_f = \Omega_{z_f} + \Omega_{x_f} f_f \quad (37)$$
$$\psi'_f = \psi_{z_f} + \psi_{x_f} f_f. \quad (38)$$

The sweep method is used to solve the neighboring extremal equations. This method offers greater stability for numerical computation than a transition matrix solution [1]. The symmetry of the coefficient matrix in Eq. (34) motivates the solution

$$\begin{bmatrix} \tilde{\delta}p \\ \delta\psi \\ \delta\Omega \end{bmatrix} = \begin{bmatrix} S(z) & R(z) & m(z) \\ R^T(z) & Q(z) & n(z) \\ m^T(z) & n^T(z) & l(z) \end{bmatrix} \begin{bmatrix} \tilde{\delta}x \\ \delta\mu \\ \delta z_f \end{bmatrix} \quad (39)$$

where the final values of these sweep variables are

$$S_f = G_{x_f x_f},\quad R_f = \psi_{x_f}^T,\quad m_f = \Omega_{x_f}^T$$
$$Q_f = 0,\quad n_f = \psi'_f,\quad l_f = \Omega'_f. \quad (40)$$

Eq. (39) is differentiated with respect to z and $\tilde{\delta}x'$, $\tilde{\delta}p'$ and $\tilde{\delta}p$ are eliminated using Eqs. (23), (24) and (34). The resulting differential equations for the sweep variables are

$$S' = -SA - A^T S + SBS - C \quad (41)$$
$$R' = (SB - A^T)R \quad (42)$$
$$m' = (SB - A^T)m \quad (43)$$
$$Q' = R^T B R \quad (44)$$
$$n' = R^T B m \quad (45)$$
$$l' = m^T B m. \quad (46)$$

The differential equation for S is a matrix Ricatti equation while the equations for R and m are linear matrix equations. The differential equations for Q, n, and l are simply quadratures. Each of the sweep variables is integrated backwards from z_f to z_0.

The Lagrange multiplier perturbations are obtained by eliminating $\delta\mu$ and δz_f from Eq. (39) to obtain

$$\tilde{\delta}p = \left[(\overline{S} - \overline{R}\,\overline{Q}^{-1}\overline{R}^T)\tilde{\delta}x + \overline{R}\,\overline{Q}^{-1}\delta\psi\right] \quad (47)$$

where $\overline{S}$, $\overline{Q}$ and $\overline{R}$ are defined as

$$\overline{S} \triangleq S - \frac{mm^T}{l} \quad (48)$$
$$\overline{Q} \triangleq Q - \frac{nn^T}{l} \quad (49)$$
$$\overline{R} \triangleq R - \frac{mn^T}{l}. \quad (50)$$

The above expression for $\tilde{\delta}p$ is used in Eq. (22) to obtain the control perturbation

$$\tilde{\delta}\bar{u} = -\left\{\left[H_{\bar{u}x} + f_{\bar{u}}^T(\overline{S} - \overline{R}\,\overline{Q}^{-1}\overline{R}^T)\right]\tilde{\delta}x + \left[f_{\bar{u}}^T \overline{R}\,\overline{Q}^{-1}\right]\delta\psi\right\} H_{\bar{u}\bar{u}}^{-1}. \quad (51)$$

This control is added to the extremal control to guide the vehicle along the neighboring extremal path.

Hypersonic Glider Problem

The above technique is now applied to maximize the final velocity of a hypersonic glider that is descending between two altitudes. The differential equations that describe a nonthrusting vehicle moving over a spherical, non-rotating Earth and modeled as a point mass are [4]

$$\frac{dX}{dt} = V\frac{r_s}{r_s + h}\cos\gamma\cos\chi \quad (52)$$
$$\frac{dY}{dt} = V\frac{r_s}{r_s + h}\cos\gamma\sin\chi \quad (53)$$
$$\frac{dh}{dt} = V\sin\gamma \quad (54)$$

$$\frac{dV}{dt} = -\frac{D}{m_0} - g_s\left(\frac{r_s}{r_s+h}\right)^2 \sin\gamma \quad (55)$$

$$\frac{d\gamma}{dt} = \frac{L}{m_0 V} + \left[\frac{V}{r_s+h} - \frac{g_s}{V}\left(\frac{r_s}{r_s+h}\right)^2\right]\cos\gamma \quad (56)$$

$$\frac{d\chi}{dt} = \frac{S}{m_0 V\cos\gamma} + \frac{V\cos\gamma\cos\chi}{r_s+h}\tan(\frac{Y}{r_s}). \quad (57)$$

In the above equations, the states $(X, Y, h, V, \gamma, \chi)$ are the downrange, the crossrange, the altitude, the velocity of the glider, the flight path angle, and the track angle. The mean radius of the Earth and gravity at the Earth's surface have the numerical values of

$$r_s = 20,925,672 \text{ ft}, \quad g_s = 32.172 \text{ ft/sec}^2. \quad (58)$$

The glider has a mass and reference surface area of

$$m_0 = 15.52 \text{ slugs}, \quad S_R = 1.5 \text{ ft}^2. \quad (59)$$

The aerodynamic lift, drag, and side force are written in terms of nondimensional aerodynamic coefficients as

$$L = \frac{1}{2}\rho V^2 S_R C_L \quad (60)$$

$$D = \frac{1}{2}\rho V^2 S_R C_D \quad (61)$$

$$S = \frac{1}{2}\rho V^2 S_R C_S \quad (62)$$

where ρ denotes the density of the air, which is determined from interpolated data of the 1976 standard atmosphere [5]. The aerodynamic coefficients are determined by linear interpolation of wind tunnel data that is stored as a function of angle of attack, sideslip angle, the Mach number and the Reynolds number.

Approximate Model

The above equations of motion define the simulation environment (or truth model) that describes the glider. Since they are highly nonlinear, a reduction to a set of model equations must be performed in order to get an analytic solution for the optimal controls. The following approximations are considered to be valid for this problem:

- **Low Altitude Flight**
  The altitude of the glider is considered to be small compared to the radius of the Earth. Therefore, $r_s + h \cong r_s$.

- **Parabolic Drag Polar**
  The glider is assumed to be flying hypersonically throughout the trajectory so the nondimensional drag coefficient is approximated by

$$C_D \cong C_{D_0}(1 + \lambda^2 + \sigma^2) \quad (63)$$

  where $\lambda \triangleq C_L/C_L^*$ and $\sigma \triangleq C_S/C_L^*$ are the scaled lift and side force coefficients and are the aerodynamic controls for this problem. The drag polar constants are

$$C_{D_0} = 0.043, \quad C_L^* = 0.2888 \quad (64)$$

  and the maximum lift-to-drag ratio is $E^* = 3.281$.

- **Dominant Aerodynamic Forces**
  Since the glider is flying hypersonically, the aerodynamic forces are assumed to be much larger than the other terms on the right hand side of the V, γ, and χ differential equations.

- **Exponential Density**
  An analytic approximation for the air density is

$$\rho_e = \rho_s e^{-h/h_R} \quad (65)$$

  where $\rho_s = 0.0023769$ slug/ft^3 is the density at sea level and $h_R = 23,800$ ft is the density scale height chosen by fitting an exponential curve to a plot of density vs. altitude.

- **Linearized Flight Path Angle**
  The flight path angle is linearized about some flight path angle γ_0 to simplify the trigonometric functions to

$$\sin\gamma \cong a_\gamma + b_\gamma\gamma \quad (66)$$

$$\cos\gamma \cong c_\gamma + d_\gamma\gamma \quad (67)$$

$$\frac{1}{\cos\gamma} \cong e_\gamma + f_\gamma\gamma \quad (68)$$

  where the coefficients a_γ - f_γ are the Taylor series expansion coefficients. The accuracy of these angular approximations depends on the range of values of the flight path angle compared with γ_0.

The dimensional states (X, Y, h, V) are replaced with the following nondimensional variables:

$$\xi \triangleq \frac{X}{h_R} \quad (69)$$

$$\eta \triangleq \frac{Y}{h_R} \quad (70)$$

$$\omega \triangleq \frac{C_L^* S_R h_R}{2m_0}\rho(h) \quad (71)$$

$$\nu \triangleq \ln\left(\frac{V^2}{g_s r_s}\right), \quad (72)$$

and the differential equation for the nondimensional density replaces Eq. (54). In addition, the time derivative of a new integration variable z is defined as [6]

$$\frac{dz}{dt} \triangleq \frac{V\omega}{h_R}. \tag{73}$$

The value of z always increases along any trajectory (unlike γ, which is used in [7]) since its time derivative is always positive. The initial value of z is chosen to be equal to 0.

The state differential equations are now rewritten exactly as

$$\begin{aligned}
\frac{d\xi}{dz} &= \frac{(c_\gamma + d_\gamma\gamma)\cos\chi}{\omega} \\
&\quad + \left\{\frac{r_s\cos\gamma\cos\chi}{(r_s+h)\omega} - \frac{(c_\gamma + d_\gamma\gamma)\cos\chi}{\omega}\right\} && (74)\\
\frac{d\eta}{dz} &= \frac{(c_\gamma + d_\gamma\gamma)\sin\chi}{\omega} \\
&\quad + \left\{\frac{r_s\cos\gamma\sin\chi}{(r_s+h)\omega} - \frac{(c_\gamma + d_\gamma\gamma)\sin\chi}{\omega}\right\} && (75)\\
\frac{d\omega}{dz} &= -(a_\gamma + b_\gamma\gamma) \\
&\quad + \left\{\frac{h_R}{\rho}\frac{d\rho}{dh}\sin\gamma + (a_\gamma + b_\gamma\gamma)\right\} && (76)\\
\frac{d\nu}{dz} &= -\frac{(1+\lambda^2+\sigma^2)}{E^*} \\
&\quad + \left\{\frac{(1+\lambda^2+\sigma^2) - C_D/C_{D_0}}{E^*}\right. \\
&\quad \left. - \frac{2h_R g_s}{V^2\omega}\left(\frac{r_s}{r_s+h}\right)^2\sin\gamma\right\} && (77)\\
\frac{d\gamma}{dz} &= \lambda + \left\{\left[\frac{1}{r_s+h}\right.\right. \\
&\quad \left.\left. - \frac{g_s}{V^2}\left(\frac{r_s}{r_s+h}\right)^2\right]\frac{h_R\cos\gamma}{\omega}\right\} && (78)\\
\frac{d\chi}{dz} &= e_\gamma\sigma + \left\{\sigma\left[\frac{1}{\cos\gamma} - e_\gamma\right]\right. \\
&\quad \left. + \frac{h_R\cos\gamma\cos\chi}{\omega(r_s+h)}\tan\left(\frac{Y}{r_s}\right)\right\}. && (79)
\end{aligned}$$

Each of the terms in braces is small compared with the corresponding non-braced terms. Therefore, the six mismatch controls $\mathrm{w}_\xi(t)$, $\mathrm{w}_\eta(t)$, $\mathrm{w}_\omega(t)$, $\mathrm{w}_\nu(t)$, $\mathrm{w}_\gamma(t)$, and $\mathrm{w}_\chi(t)$ are defined to replace those braced terms. The model equations of motion, then, are

$$\begin{aligned}
\frac{d\xi}{dz} &= \frac{(c_\gamma + d_\gamma\gamma)\cos\chi}{\omega} + \mathrm{w}_\xi && (80)\\
\frac{d\eta}{dz} &= \frac{(c_\gamma + d_\gamma\gamma)\sin\chi}{\omega} + \mathrm{w}_\eta && (81)\\
\frac{d\omega}{dz} &= -(a_\gamma + b_\gamma\gamma) + \mathrm{w}_\omega && (82)\\
\frac{d\nu}{dz} &= -\frac{(1+\lambda^2+\sigma^2)}{E^*} + \mathrm{w}_\nu && (83)\\
\frac{d\gamma}{dz} &= \lambda + \mathrm{w}_\gamma && (84)\\
\frac{d\chi}{dz} &= e_\gamma\sigma + \mathrm{w}_\chi. && (85)
\end{aligned}$$

Guidance Scheme

A close examination of the model equations reveals that the last four equations are linear in the states (quadratic in the controls). However, the range equations, Eqs. (80) and (81), contain the state ω in the denominator. An analytic optimal control solution for the descent to a constrained downrange, crossrange, and altitude cannot be found because of this nonlinearity.

For this reason,the guidance scheme used to reach a desired location is similar to the one found in [7]. At each guidance step:

1. The linearization coefficients are recalculated based on the current state of the glider.
2. The unconstrained-range (UR) optimal controls are calculated for a descent from the current position to the constrained final altitude only.
3. The final states of the glider using the UR controls are determined by numerically integrating the necessary model differential equations.
4. The miss distance between the desired final position and the UR final location is used to calculate the NE controls (see Fig. 1). The NE corrections are added to the UR controls and applied to the vehicle.

Optimal UR Controls

The optimal control problem is to find the two sets of controls $\boldsymbol{u}$ and $\mathbf{w}$ that respectively minimize and extremize the performance index

$$J = \left[-\nu_f + \frac{1}{2}\int_o^{z_f} \mathbf{w}^T\mathbf{M}^{-1}\mathbf{w}\, dz\right] \tag{86}$$

subject to the model differential equations, Eqs. (80) - (85), and the boundary conditions

$$z_0 = 0, \quad \boldsymbol{x}_0 \text{ specified} \tag{87}$$

$$\boldsymbol{\psi}(z_f, \boldsymbol{x}_f) = \begin{bmatrix} \xi_f - \xi_D \\ \eta_f - \eta_D \\ \omega_f - \omega_D \end{bmatrix} = \mathbf{0}, \tag{88}$$

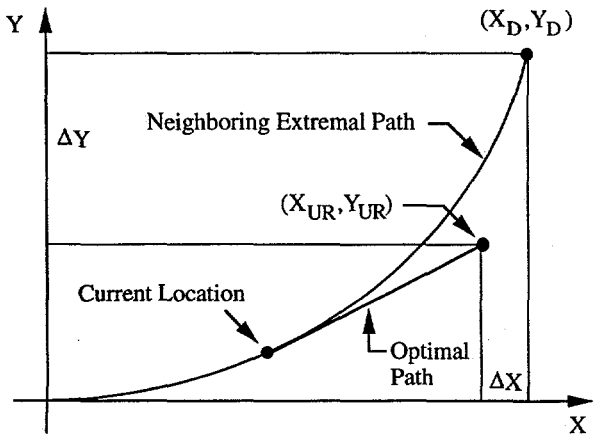

Figure 1: Neighboring extremal miss distances.

where the subscript D denotes the desired final location. The downrange and crossrange equations and constraints are included in the problem formulation only for the subsequent calculation of the NE controls.

The performance index is separable for this problem since $d\nu/dz = f_1(\boldsymbol{u}) + f_2(\mathbf{w})$ and integration is a linear operator. The Bolza function and the Hamiltonian for this problem are

$$\begin{aligned} G &= -\nu_f + \mu_\xi(\xi_f - \xi_D) \\ &\quad +\mu_\eta(\eta_f - \eta_D) + \mu_\omega(\omega_f - \omega_D) \qquad (89) \\ H &= \frac{1}{2}\left[\frac{\mathrm{w}_\xi^2}{\mathrm{M}_\xi} + \frac{\mathrm{w}_\eta^2}{\mathrm{M}_\eta} + \frac{\mathrm{w}_\omega^2}{\mathrm{M}_\omega} + \frac{\mathrm{w}_\nu^2}{\mathrm{M}_\nu} + \frac{\mathrm{w}_\gamma^2}{\mathrm{M}_\gamma} + \frac{\mathrm{w}_\chi^2}{\mathrm{M}_\chi}\right] \\ &\quad +p_\xi\left[\frac{(c_\gamma + d_\gamma\gamma)\cos\chi}{\omega} + \mathrm{w}_\xi\right] \\ &\quad +p_\eta\left[\frac{(c_\gamma + d_\gamma\gamma)\sin\chi}{\omega} + \mathrm{w}_\eta\right] \\ &\quad +p_\omega\left[-(a_\gamma + b_\gamma\gamma) + \mathrm{w}_\omega\right] \\ &\quad +p_\nu\left[-\frac{(1+\lambda^2+\sigma^2)}{E^*} + \mathrm{w}_\nu\right] \\ &\quad +p_\gamma\left[\lambda + \mathrm{w}_\gamma\right] + p_\chi\left[e_\gamma\sigma + \mathrm{w}_\chi\right]. \qquad (90) \end{aligned}$$

Since the ranges are not constrained, the associated Lagrange multipliers are set to zero, i.e. $\mu_\xi = \mu_\eta = 0$ and $p_\xi = p_\eta = 0$. From Eqs. (4) and (11), the other multipliers are

$$\begin{aligned} p_\omega &= \text{unknown constant} \qquad (91) \\ p_\nu &= -1 \qquad (92) \\ p_\gamma &= b_\gamma p_\omega(z - z_f) \qquad (93) \\ p_\chi &= 0. \qquad (94) \end{aligned}$$

The extremal UR controls are determined from Eqs. (5) and (6) to be

$$\begin{aligned} \lambda_{UR} &= -\frac{E^*}{2} b_\gamma p_\omega(z - z_f) \qquad (95) \\ \sigma_{UR} &= 0 \qquad (96) \\ \mathrm{w}_\xi &= 0 \qquad (97) \\ \mathrm{w}_\eta &= 0 \qquad (98) \\ \mathrm{w}_\omega &= -p_\omega \mathrm{M}_\omega \qquad (99) \\ \mathrm{w}_\nu &= \mathrm{M}_\nu \qquad (100) \\ \mathrm{w}_\gamma &= -b_\gamma p_\omega \mathrm{M}_\gamma(z - z_f) \qquad (101) \\ \mathrm{w}_\chi &= 0 \qquad (102) \end{aligned}$$

using the above expression for p_γ. Both σ and w_χ are zero, which implies that the UR descent occurs in a vertical plane. The aerodynamic controls satisfy the Legendre-Clebsch condition since

$$H_{\lambda\lambda} = H_{\sigma\sigma} = -\frac{2p_\nu}{E^*} > 0. \qquad (103)$$

The unknowns p_ω and z_f are determined by analytically integrating Eq. (84), then Eq. (82), and then applying the first integral (for details, see [8]). The expression for p_ω in terms of z_f is

$$p_\omega = \frac{c_1 + \sqrt{c_1^2 - 2K_\nu c_2}}{c_2} \qquad (104)$$

where

$$\begin{aligned} c_1 &\triangleq a_\gamma + b_\gamma\gamma_0 + b_\gamma\bar{\mathcal{M}}_0 z_f \qquad (105) \\ c_2 &\triangleq -\mathrm{M}_\omega - b_\gamma^2 K_\gamma z_f^2 \qquad (106) \end{aligned}$$

and the constants K_ν and K_γ are defined as

$$\begin{aligned} K_\nu &\triangleq \frac{1}{E^*} + \frac{M_\nu}{2} \qquad (107) \\ K_\gamma &\triangleq M_\gamma - \frac{E^*}{2}. \qquad (108) \end{aligned}$$

The value of z_f is a root of the sixth-order polynomial

$$a_6 z_f^6 + a_4 z_f^4 + a_3 z_f^3 + a_2 z_f^2 + a_0 = 0 \qquad (109)$$

whose coefficients are

$$\begin{aligned} a_6 &= b_\gamma^4\left[8K_\nu K_\gamma^2 + 3K_\gamma\bar{\mathcal{M}}_0^2\right] \qquad (110) \\ a_4 &= b_\gamma^2\mathrm{M}_\omega\left[48K_\nu K_\gamma + 27\bar{\mathcal{M}}_0^2\right] \\ &\quad -12K_\gamma\left[b_\gamma^3\bar{\mathcal{M}}_0\Delta\omega + b_\gamma^4\gamma_0^2\right. \\ &\quad \left. +a_\gamma^2 b_\gamma^2 + 2a_\gamma b_\gamma^3\gamma_0\right] \qquad (111) \\ a_3 &= 72\bar{\mathcal{M}}_0\mathrm{M}_\omega\left[b_\gamma^2\gamma_0 + a_\gamma b_\gamma\right] \\ &\quad -48K_\gamma\Delta\omega\left[b_\gamma^3\gamma_0 + a_\gamma b_\gamma^2\right] \qquad (112) \\ a_2 &= 72K_\nu\mathrm{M}_\omega^2 - 36b_\gamma^2 K_\gamma\Delta\omega^2 \\ &\quad +36\mathrm{M}_\omega\left[b_\gamma\bar{\mathcal{M}}_0\Delta\omega + b_\gamma^2\gamma_0^2\right. \\ &\quad \left. +2a_\gamma b_\gamma\gamma_0 + a_\gamma^2\right] \qquad (113) \\ a_0 &= -36\Delta\omega^2\mathrm{M}_\omega. \qquad (114) \end{aligned}$$

Simulation work reveals that the correct value of z_f is the second positive root of Eq. (109). This value must be determined numerically since there is no known analytical solution to a sixth-order polynomial.

Neighboring Extremal Controls

The NE trajectory is defined relative to the UR path. Therefore, all of the partial derivatives and sweep variables used for the NE control computation are evaluated on the extremal path along which $p_\xi = p_\eta = 0$.

The boundary conditions for the sweep variables are determined from Eq. (40) to be

$$\boldsymbol{S}_f = \mathbf{0}_{6\times 6}, \quad \boldsymbol{Q}_f = \mathbf{0}_{6\times 6}, \quad l_f = -b_\gamma \bar{\mathcal{M}}_0 p_\omega \tag{115}$$

$$\boldsymbol{R}_f = \begin{bmatrix} 1 & 0 & 0 \\ 0 & 1 & 0 \\ 0 & 0 & 1 \\ 0 & 0 & 0 \\ 0 & 0 & 0 \\ 0 & 0 & 0 \end{bmatrix}, \quad \boldsymbol{m}_f = \begin{bmatrix} 0 \\ 0 \\ 0 \\ 0 \\ -b_\gamma p_\omega \\ 0 \end{bmatrix} \tag{116}$$

$$\boldsymbol{n}_f = \begin{bmatrix} \dfrac{(c_\gamma + d_\gamma \gamma_f)\cos\chi_f}{\omega_f} \\ \dfrac{(c_\gamma + d_\gamma \gamma_f)\sin\chi_f}{\omega_f} \\ -(a_\gamma + b_\gamma \gamma_f) - p_\omega \mathrm{M}_\omega \end{bmatrix}. \tag{117}$$

These final conditions are used to integrate the differential equations describing the sweep variables backwards from z_f to $z_0 \triangleq 0$.

The differential equation for $\boldsymbol{S}$ is homogeneous since $\boldsymbol{C} = \mathbf{0}_{6\times 6}$. Therefore, since $\boldsymbol{S}_f$ is zero,

$$\boldsymbol{S}(z) = \mathbf{0}_{6\times 6}. \tag{118}$$

The derivative of the $\boldsymbol{R}$ matrix is defined in Eq. (42). Solving for those elements of $\boldsymbol{R}$ that can be integrated yields

$$\boldsymbol{R}(z) = \begin{bmatrix} 1 & 0 & 0 \\ 0 & 1 & 0 \\ R_{31} & R_{32} & 1 \\ 0 & 0 & 0 \\ R_{51} & R_{52} & b_\gamma(z - z_f) \\ R_{61} & R_{62} & 0 \end{bmatrix}. \tag{119}$$

The remaining elements have the following differential equations:

$$\frac{dR_{31}}{dz} = \frac{(c_\gamma + d_\gamma\gamma)\cos\chi}{\omega^2} \tag{120}$$

$$\frac{dR_{32}}{dz} = \frac{(c_\gamma + d_\gamma\gamma)\sin\chi}{\omega^2} \tag{121}$$

$$\frac{dR_{51}}{dz} = \frac{-d_\gamma\cos\chi}{\omega} + b_\gamma R_{31} \tag{122}$$

$$\frac{dR_{52}}{dz} = \frac{-d_\gamma\sin\chi}{\omega} + b_\gamma R_{32} \tag{123}$$

$$\frac{dR_{61}}{dz} = \frac{(c_\gamma + d_\gamma\gamma)\sin\chi}{\omega} \tag{124}$$

$$\frac{dR_{62}}{dz} = \frac{-(c_\gamma + d_\gamma\gamma)\cos\chi}{\omega}. \tag{125}$$

The $\boldsymbol{Q}$ matrix is symmetric since its derivative, defined in Eq. (44), is symmetric and $\boldsymbol{Q}_f = \mathbf{0}$. The differential equations for the first 5 elements of $\boldsymbol{Q}$ are

$$\frac{dQ_{11}}{dz} = \mathrm{M}_\xi + R_{31}^2\mathrm{M}_\omega + K_\gamma R_{51}^2 + K_\chi R_{61}^2 \tag{126}$$

$$\frac{dQ_{12}}{dz} = R_{31}R_{32}\mathrm{M}_\omega + K_\gamma R_{51}R_{52} + K_\chi R_{61}R_{62} \tag{127}$$

$$\frac{dQ_{13}}{dz} = R_{31}\mathrm{M}_\omega + b_\gamma K_\gamma R_{51}(z - z_f) \tag{128}$$

$$\frac{dQ_{22}}{dz} = \mathrm{M}_\eta + R_{32}^2\mathrm{M}_\omega + K_\gamma R_{52}^2 + K_\chi R_{62}^2 \tag{129}$$

$$\frac{dQ_{23}}{dz} = R_{32}\mathrm{M}_\omega + b_\gamma K_\gamma R_{52}(z - z_f) \tag{130}$$

where

$$K_\chi \triangleq \mathrm{M}_\chi + e_\gamma^2 \frac{E^*}{2}. \tag{131}$$

The last diagonal element of Q is integrated to be

$$Q_{33}(z) = M_\omega(z - z_f) + b_\gamma^2 K_\gamma \left(\frac{z^3}{3} - z_f z^2 + z_f^2 z - \frac{z_f^3}{3} \right). \tag{132}$$

The $\boldsymbol{m}$ matrix is constant and $\boldsymbol{m}(z) = \boldsymbol{m}_f$. The derivatives of the first two elements of the $\boldsymbol{n}$ matrix are

$$\frac{dn_1}{dz} = -b_\gamma K_\gamma p_\omega R_{51} \tag{133}$$

$$\frac{dn_2}{dz} = -b_\gamma K_\gamma p_\omega R_{52}, \tag{134}$$

and the third element of the matrix is

$$n_3(z) = -b_\gamma^2 K_\gamma p_\omega \left(\frac{z^2}{2} - z_f z + \frac{z_f^2}{2} \right) - (a_\gamma + b_\gamma\gamma_f) + \frac{p_\omega}{\mathrm{M}_\omega}. \tag{135}$$

Finally, the sweep variable l is

$$l(z) = b_\gamma^2 K_\gamma p_\omega^2 (z - z_f). \tag{136}$$

The sweep variables are used to calculate the neighboring extremal control perturbations from Eqs. (48) - (51). The thirteen differential equations for the matrix elements that are listed above must be integrated numerically.

Numerical Results

The UR optimal controls are added to the NE corrections to obtain the total aerodynamic controls

$$\lambda = -\frac{E^*}{2} b_\gamma p_\omega (z - z_f) + \tilde{\delta}\lambda \qquad (137)$$

$$\sigma = \tilde{\delta}\sigma \qquad (138)$$

which are applied to the vehicle. These commanded controls are assumed to be instantaneously achievable. At each guidance step during the simulation (every 0.1 seconds), the linearization coefficients and the controls are computed and held constant until the next guidance step.

Neither the mismatch controls nor their NE perturbations enter directly in the simulation environment since they do not appear explicitly in the simulation equations of motion. However, they are included implicitly throughout the problem in the equation for p_ω, the equations for the coefficients $a_0, a_2, \ldots, a_6$, and the NE sweep variable differential equations.

The glider is initially flying at a constant altitude of 100,000 ft with a flight path angle of 0°. The initial velocity of the vehicle is 11,000 ft/sec and both the initial time and downrange are set to zero. Depending on the values of the tuning parameters, the UR trajectory to a final altitude is 0 ft ends at a downrange of about 70 nm and exactly no crossrange. The first scenario that is examined is the descent to a downrange of 70 nm and a crossrange of 10 nm.

Four control laws are used to guide the vehicle. The first two are of the form derived in this paper but use different values of the tuning parameters. The *untuned* controller has all of the tuning parameters set to 0, which corresponds to zero mismatch controls. The *tuned* controller uses a suboptimal set of tuning parameters chosen by testing various combinations of parameter values. The only parameters changed from 0 for this tuned set are $M_\omega = 1/500$ and $M_\nu = 1$. The third control law is a seven-node piecewise-linear control law determined by a numerical parameter optimization code using the true vehicle dynamics [9]. The last control law is a proportional navigation (PRONAV) scheme that weights the final miss distance ten times more than the integrated square control effort [8].

Unfortunately, the determinant of the sweep variable Q decreases tremendously along the trajectory for both sets of the tuning parameters (see Fig. 2). The small determinant causes the NE control corrections to get very large, since they are a function of Q^{-1}. To avoid the misleading large decrease in the final velocity due to large terminal controls, PRONAV is used in place of the tuned and untuned control laws after the glider passes 10,000 ft altitude, which corresponds roughly to the last

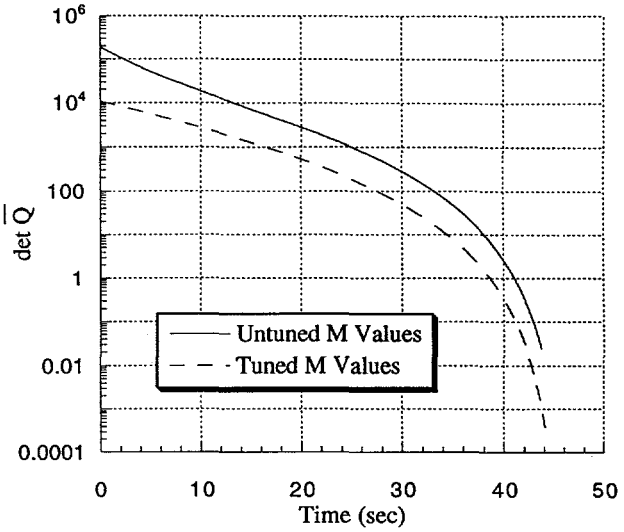

Figure 2: The determinant of the sweep variable $\bar{Q}$.

2 seconds of the trajectory. The switch to PRONAV is justified by the fact that the glider is essential pointing directly at the desired final position at 10,000 ft altitude and very little control effort is needed to achieve the desired final position.

The commanded lift and side force coefficients generated by the four control laws are compared in Figs. 3 and 4. For both the lift and the side force, the tuning procedure modifies the controls to be more like the numerically-determined optimal control. The tuned side force coefficient does not match the numerical optimal control as well as the lift coefficient because the crossrange control is achieved only by the neighboring extremal control.

All of the control laws successfully guide the vehicle to the desired final location. The trajectories that the glider follows using these control laws are shown in Figs. 5 and 6 and the final velocities of the glider are listed in Table 1. PRONAV yields the lowest final velocity which is to be expected since it minimizes the miss distance (relative to the control effort) and not the final velocity. For the controller derived in this paper, the tuning procedure increases the final velocity over 250 ft/sec. In addition, the final velocity using the tuned

Table 1: Performance comparison of the controllers.

	V_f (ft/sec)
Untuned Controller	6517.6
Tuned Controller	6780.4
Numerical Optimal	6798.7
PRONAV	4767.0

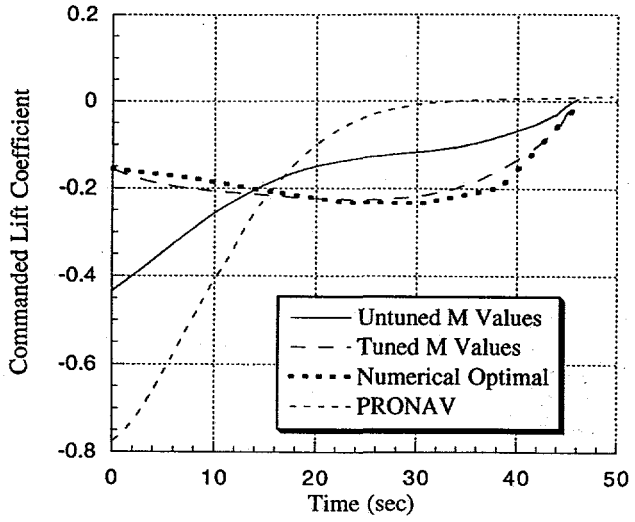

Figure 3: Comparison of commanded C_L.

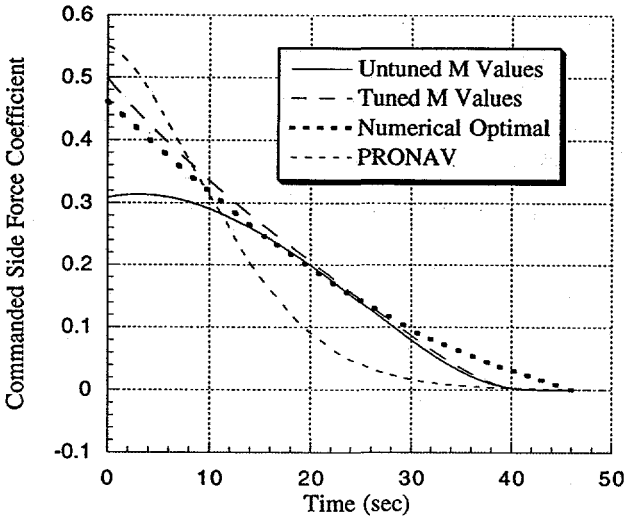

Figure 4: Comparison of commanded C_S.

controller is within 20 ft/sec of the velocity produced using the numerical optimal control law.

The altitude profile of the glider using the tuned control law is almost coincident with the numerical-determined profile. However, the groundtracks using the tuned and untuned controllers are equally far from the groundtrack produced using the numerical optimal control law. This situation arises because the UR optimal side force control is identically zero and the crossrange is achieved solely with the NE control. The tuning procedure is therefore more effective when the UR control has a specific form about which the NE controls can be linearized.

A comparison of the tuned and untuned control laws for different desired final locations is shown in Figs. (7) and (8) . Both controllers guide the vehicle to the desired final locations and the tuned controller consistently outperforms the untuned controller. The performance gain of the tuned controller does decrease as the final position gets farther from the design point about which the parameters were tuned.

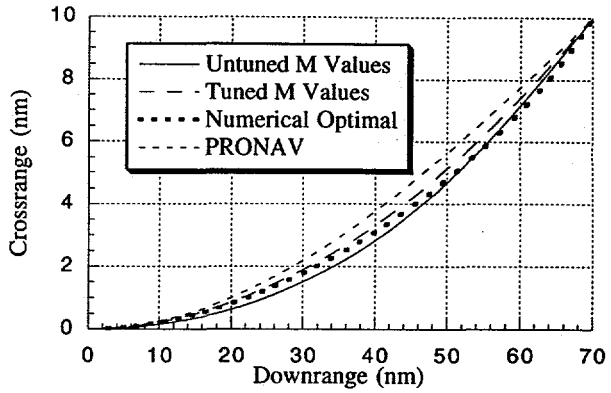

Figure 5: Groundtracks for the three controllers.

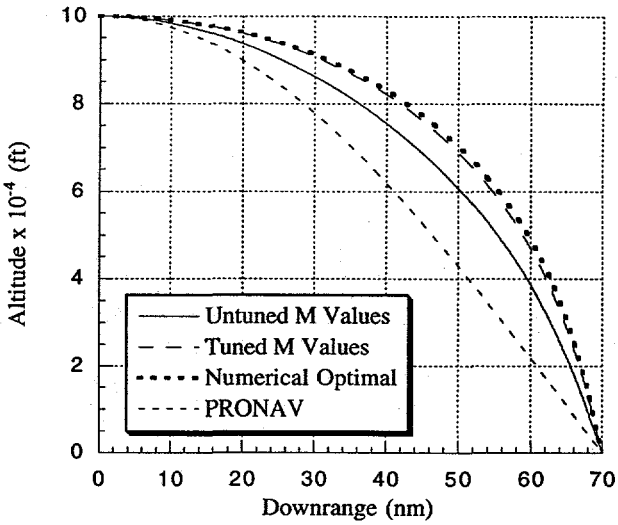

Figure 6: Altitude profiles for the controllers.

Conclusions

The neighboring extremal controls have been derived for a system that includes mismatch controls to simplify the model equations of motion. The tuning parameters associated with the mismatch controls are adjusted after the neighboring extremal controls are added to the extremal controls and simulated on a computer. The specific example shows that the performance of the tuned control law approaches the performance achieved using a numerically-determined piecewise-linear controller and is much better than the performance obtained using a proportional navigation control law.

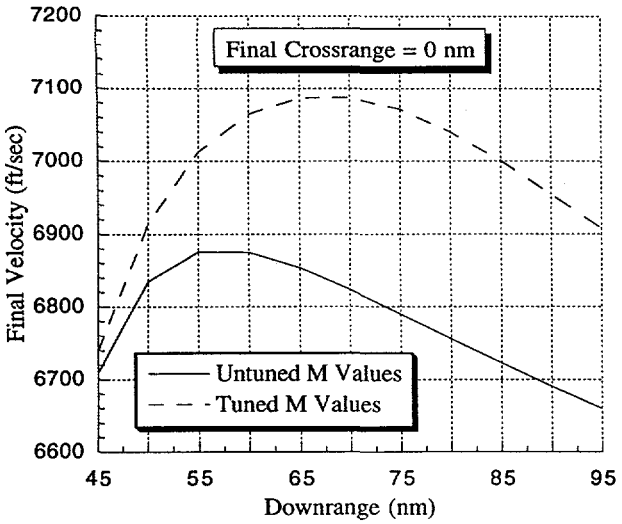

Figure 7: Performance comparisons for crossranges.

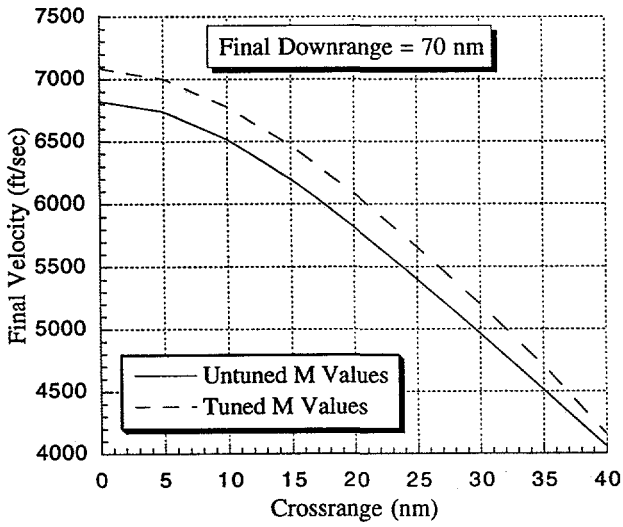

Figure 8: Performance comparisons for downranges.

Acknowledgement

This work was supported in part by the Department of Energy under Contract DE-AC04-94AL-85000.

References

[1] Bryson, A. E., and Ho, Y. C. *Applied Optimal Control.* Hemisphere Publishing Corporation, 1975.

[2] Kim, T. J., and Hull, D. G. "An Optimal Control Design that Accounts for Model Mismatch Errors." AAS/AIAA Space Flight Mechanics Meeting, Albuquerque, New Mexico, February, 1995.

[3] Isaacs, R. *Differential Games.* Robert E. Krieger Publishing Co., 1975.

[4] Feeley, T. S., and Speyer, J. L. "A Real-Time Approximate Optimal Guidance Law for Flight in a Plane." Proceedings of the 1990 American Control Conference, San Diego, California, May 1990.

[5] United States Committee on Extension to the Standard Atmosphere *U. S. Standard Atmosphere.* Washington, D.C., 1976.

[6] Speyer, J. L., and Crues, E. Z. "Approximate Optimal Atmospheric Guidance Law for Aeroassisted Plane-Change Maneuvers." Journal of Guidance, Control, and Dynamics, Vol. 13, No. 5, Sept/Oct 1990.

[7] Eisler, G. R., and Hull, D. G. "Guidance Law for Hypersonic Descent to a Point." Journal of Guidance, Control, and Dynamics, Vol. 17, No. 4, Jul/Aug 1994.

[8] Kim, T. J. *A Mixed Nonlinear/Linear Control Design for Optimal Descent Trajectories.* Ph.D. Thesis, The University of Texas, 1994.

[9] Lasdon, L. S. and Waren, A. D. *GRG2 User's Guide.* 1989.